Thermoelectric properties of Pb and Na dual doped BiCuSeO

Cite as: AIP Advances **9**, 015025 (2019); https://doi.org/10.1063/1.5066296
Submitted: 14 October 2018 . Accepted: 15 January 2019 . Published Online: 24 January 2019

Sayan Das, Suneesh Meledath Valiyaveettil, Kuei-Hsien Chen, Satyam Suwas, and Ramesh Chandra Mallik

Thermoelectric properties of Pb and Na dual doped BiCuSeO

Cite as: AIP Advances 9, 015025 (2019); doi: 10.1063/1.5066296
Submitted: 14 October 2018 • Accepted: 15 January 2019 •
Published Online: 24 January 2019

Sayan Das,[1] Suneesh Meledath Valiyaveettil,[2] Kuei-Hsien Chen,[2] Satyam Suwas,[3] and Ramesh Chandra Mallik[1,a)]

AFFILIATIONS

[1]Thermoelectric Materials and Devices Laboratory, Department of Physics, Indian Institute of Science, Bangalore, India
[2]Institute of Atomic and Molecular Sciences, Academia Sinica, No. 1, Sec. 4, Roosevelt Road, Taipei, Taiwan
[3]Department of Materials Engineering, Indian Institute of Science, Bangalore 560012, India

[a)]**Corresponding author's phone no:** +918022932450, **Electronic mail:** rcmallik@iisc.ac.in

ABSTRACT

BiCuSeO is a promising thermoelectric material not only because of its good thermoelectric properties, but also earth abundant constituents. In this report, Pb and Na have been simultaneously doped at the Bi site of BiCuSeO. Doping Pb is beneficial for the Seebeck coefficient whereas doping Na maintains the hole mobility. Both the dopants increase the carrier concentration and reduce the thermal conductivity by point-defect scattering. The samples with nominal composition $Bi_{0.985-x}Na_{0.015}Pb_xCuSeO$ (x=0.00, 0.04, 0.06 and 0.08) were prepared using two-step solid-state synthesis. The X-ray diffraction pattern reveals a small amount of $Bi_2O_{2.5}$ phase (<1 vol. %) which is responsible for adversely affecting the electrical conductivity of all the samples. Both the Seebeck coefficient and electrical resistivity decrease with increasing doping fraction due to increasing hole concentration. The highest power factor of 530 $\mu W/mK^2$ was obtained for $Bi_{0.905}Na_{0.015}Pb_{0.08}CuSeO$ sample at 773 K because of moderate Seebeck coefficient and low electrical resistivity. A low lattice thermal conductivity of 0.37 W/m-K at 773 K was obtained in the $Bi_{0.905}Na_{0.015}Pb_{0.08}CuSeO$. Due to this low lattice thermal conductivity combined with the high power factor, a zT of 0.63 was obtained for the $Bi_{0.905}Na_{0.015}Pb_{0.08}CuSeO$ sample at 773 K.

I. INTRODUCTION

Thermoelectricity converts heat directly into electricity and vice-versa. The conversion efficiency of such system is governed by the dimensionless thermoelectric figure of merit (zT) of the material, which is given by-

$$zT = \frac{S^2}{\rho\kappa}T, \quad (1)$$

where S the Seebeck coefficient, ρ the electrical resistivity, κ the thermal conductivity and T is the temperature. The aim of the research in thermoelectricity is to increase the efficiency of the device by increasing the zT of TE material. Along with high zT, the oxidation resistance and the stability are the major issues for the thermoelectric materials in mid to high temperature (>600 K) applications. Bismuth oxy-selenide is a *p*-type thermoelectric material which has good stability at high temperatures and is fairly oxidation resistant up to 573 K.[1] It has favorable transport properties like moderately high S (350-425 μV/K in 300-923 K), and ultra-low κ (0.62-0.42 W/m-K in 300-923 K). However, the ρ is high (10-0.67 mΩ-m in 300-923 K) due to a low charge carrier concentration of ~$10^{18}/cm^3$, which limits the zT to 0.5 at 923 K.[2] High zTs (>1) have been obtained in BiCuSeO by doping Ba (1.1 at 923 K)[3] or Pb (1.14 at 823 K)[4] at the Bi site. The $6S^2$ lone pair electrons of Pb introduces states near the Fermi level which is advantageous for the S. However, the optimally Pb-doped BiCeSeO does not reach to the charge carrier concentration of $10^{21}/cm^3$, since its solubility is limited to 6-8 at. %.[4] Hence, there is scope to further increase the charge carrier concentration of the Pb-doped BiCuSeO by dual doping. This can be accomplished by doping another element along with Pb. For example, simultaneous doping of Ca, Pb leads to a zT of 1.5 at

873 K which is the highest zT achieved till date in BiCuSeO.[5] However, dual doping can severely reduce the already low hole mobility of BiCuSeO (~10 $cm^2/V\text{-}s$)[4] by lattice distortion induced charge scattering. The similar atomic radii of Na^+ (0.96 Å) and Bi^{+3} (0.97 Å) results in lower lattice-distortion and hence higher hole-mobility in Na-doped BiCuSeO in comparison to the other dopants like Ba.[6] Thus, Na has been doped simultaneously with Pb at the Bi site in this study. Both the dopants increase the hole concentration. The mass difference between the host Bi atoms and the dopants (Pb and Na) can decrease the lattice thermal conductivity (κ_L). The doping fraction of Na was fixed to the optimized value of 1.5 at. %[6] and the doping fraction of Pb was varied according to the composition $Bi_{0.985-x}Na_{0.015}Pb_xCuSeO$ (x=0, 0.04, 0.06 and 0.08). Due to low ρ, and moderate S, a high power factor of 530 μW/m-K^2 was achieved in $Bi_{0.905}Na_{0.015}Pb_{0.08}CuSeO$ sample at 773 K. The improved power factor and the reduced κ_L resulted in a maximum zT of 0.63 at 773 K.

II. EXPERIMENTAL DETAILS

Bi_2O_3, Cu, Se, Bi, $NaNO_2$ powders and finely cut Pb sheet were taken in a stoichiometric ratio according to the composition $Bi_{0.985-x}Na_{0.015}Pb_xCuSeO$ (x=0, 0.04, 0.06 and 0.08). The samples were synthesized using standard two-step solid-state synthesis involving furnace reaction and hot press (the details can be found elsewhere[7]). The density of the pressed pellets was more than 95% of the theoretical density as measured by the Archimedes principle. The X-ray diffraction (XRD) was carried out in a Rigaku Smartlab diffraction system having a Cu Kα source (λ = 1.54187 Å). The Fullprof software was used for the Rietveld refinement of the diffraction patterns.[8] A FEI ESEM-Quanta 200 scanning electron microscope was used for surface morphology studies. Electron probe microanalysis (EPMA) was performed in JEOL JXA8230 instrument. The Hall measurement was performed using a home-grown setup using an electromagnet with 0.7 T field strength. Keithley 6221 was used as a current source and Keithley 2182 nanovoltmeter was used to measure the voltage. Delta configuration was used to cancel out the thermal voltages. The S and the ρ of the bar-shaped samples (~11.8×1.8×1.1 mm^3) were simultaneously measured in the Linseis LSR-3 system from 373K to 773 K. The thermal diffusivity (D) and the specific heat capacity (C_p) of the cylindrical samples (diameter =10 mm, thickness ~1 mm) were measured using the laser flash apparatus LFA 457 MicroFlash. The κ was calculated using the formula $\kappa = DdC_p$ where d is the density of the samples. The errors in the measurement of the S, ρ, and the κ are 7%, 10%, and 6% respectively.

III. COMPUTATIONAL DETAILS

The density functional theory (DFT) calculation was performed using the Quantum Espresso (QE) software package.[9] Calculations were done in a 3×3×1 super cell (72 atoms), containing one Bi atom replaced by one Na atom. The plane-wave energy cutoff was 60 Ry and the electronic energy convergence was set at 10^{-8} eV. The exchange-correlation energy was approximated using Perdew–Burke–Ernzerhof (PBE) functional and generalized gradient approximation (GGA) with projector augmented wave (PAW) method.[10] The Brillouin zone was sampled by Monkhorst–Pack (MP) special k-point scheme (Γ-centered) with 4×4×3 k-point meshes. The force convergence for ions was set to 10^{-3} eV/Å for variable-cell structure relaxation.

IV. RESULTS AND DISCUSSIONS

A. X-ray diffraction pattern

The X-ray diffraction patterns of the samples is shown in Figure 1. The major peaks were matched to the standard data of BiCuSeO (ICDD card no. 04-007-6446) which confirmed the crystal structure (tetragonal, space group $P4/nmm$) of BiCuSeO. A trace amount of $Bi_2O_{2.5}$ phase (ICDD card no. 04-005-5135) was found for all the samples. Rietveld refinement was performed to retrieve the crystallographic and phase information. Figure 2 shows the Rietveld refinement result for the $Bi_{0.925}Na_{0.015}Pb_{0.06}CuSeO$, comparing the experimental and simulated curves. The volume percentage of the $Bi_2O_{2.5}$ phase, from the refinement is 0.62, 0.66, 0.85 and 0.67 for x=0.0, 0.04, 0.06 and 0.08 respectively. Repeated synthesis of the material was carefully performed to eliminate the secondary phase, but it the $Bi_2O_{2.5}$ could not be completely removed. The lattice parameters, as a function of doping percentage, obtained from Rietveld refinement is shown in the inset of Figure 2. Both the '*a*' and '*c*' increases with increasing Pb content. The ionic radius of Pb^{+2} (1.19 Å) is more than that of the Bi^{+3} (0.97 Å) hence, the '*a*' axis increases with increasing doping percentage.[10] Since the $(Bi_2O_2)^{+2}$ and the $(Cu_2Se_2)^{-2}$ have opposite charges on the layers, the two layers are coupled by coulomb force. The doping of Pb at the Bi site produces hole which is transferred to the $(Cu_2Se_2)^{-2}$ layer. The Coulomb coupling gets weaker as the charge on both the layers decreases due to hole transfer. This weaker Coulomb coupling manifests in increased '*c*' parameter.

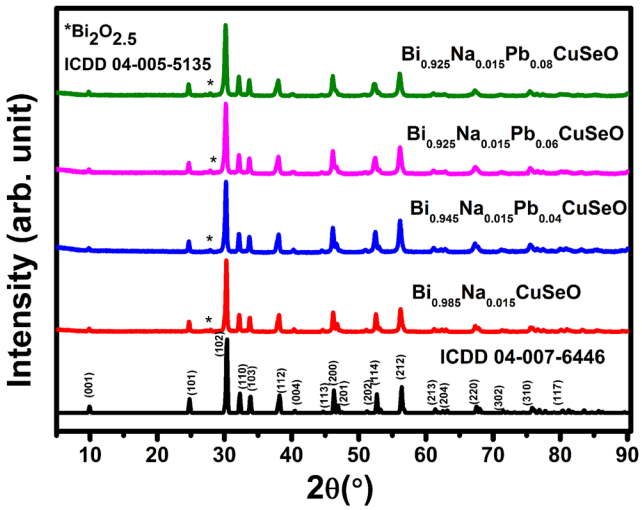

FIG. 1. X-ray diffraction pattern of the $Bi_{0.985-x}Na_{0.015}Pb_xCuSeO$ (x=0, 0.04, 0.06 and 0.08) samples compared with the standard data of BiCuSeO (ICDD card no. 04-007-6446).

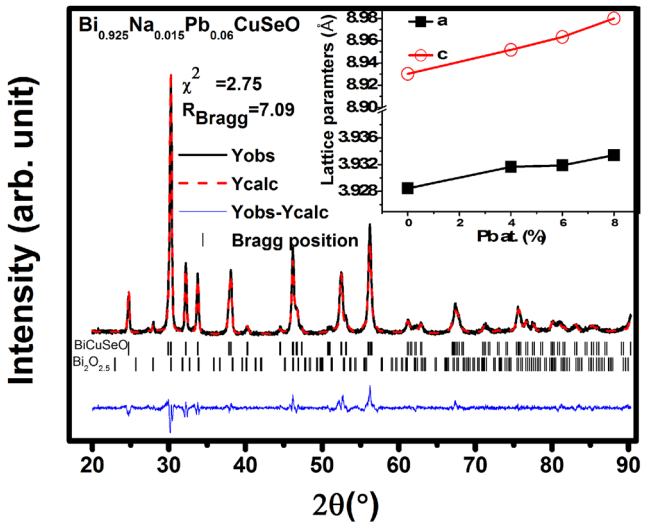

FIG. 2. The Rietveld refinement of the sample $Bi_{0.925}Pb_{0.06}Na_{0.015}CuSeO$. The black continuous line represents the experimental data, the red dashed line represents the simulated data, the blue line in the bottom represents the difference between the experimental data and the simulated data. The vertical black lines on the top and bottom represent the Bragg positions of BiCuSeO and $Bi_2O_{2.5}$ respectively. The inset shows the lattice parameter variation with doping of Pb.

B. Scanning electron microscopy and compositional analysis

The back scattered electron (BSE) image and the corresponding secondary electron (SE) image of the polished surface of the samples is shown in Figure 3. The black spots in the images corresponds to surface pits, and no phase contrast for the $Bi_2O_{2.5}$ phase was observed, probably because of its low volume fraction. The SE image of the fractured surface of the samples is shown in Figure 4. The size of the particles in the microstructure varied from below 1 μm to few μm in sizes. The densely packed particle is indicative of high density of the sample (>95% of the theoretical density). The Bi, Cu, Pb and Na content of the sample obtained from EPMA is shown in Table I. All the samples show a slightly lower Bi content than the nominal composition, which is due to the formation of $Bi_2O_{2.5}$ secondary phase. The Na content of the samples is underestimated because of lack of standard as well as low atomic number of Na. The Pb content in the $Bi_{0.905}Pb_{0.08}Na_{0.015}CuSeO$ sample is lower than the nominal composition which because of the onset of solubility limit of Pb at the Bi site.

C. Hall measurement

The Hall measurement was performed for the $Bi_{0.985}Na_{0.015}CuSeO$, $Bi_{0.945}Na_{0.015}Pb_{0.04}CuSeO$ and $Bi_{0.925}Na_{0.015}Pb_{0.06}CuSeO$ samples. Hall measurement of the $Bi_{0.905}Na_{0.015}Pb_{0.08}CuSeO$ sample could not be performed because of low signal to noise ratio owing to its high carrier concentration. This is evident from the fact that it has lower Seebeck coefficient and electrical resistivity than the

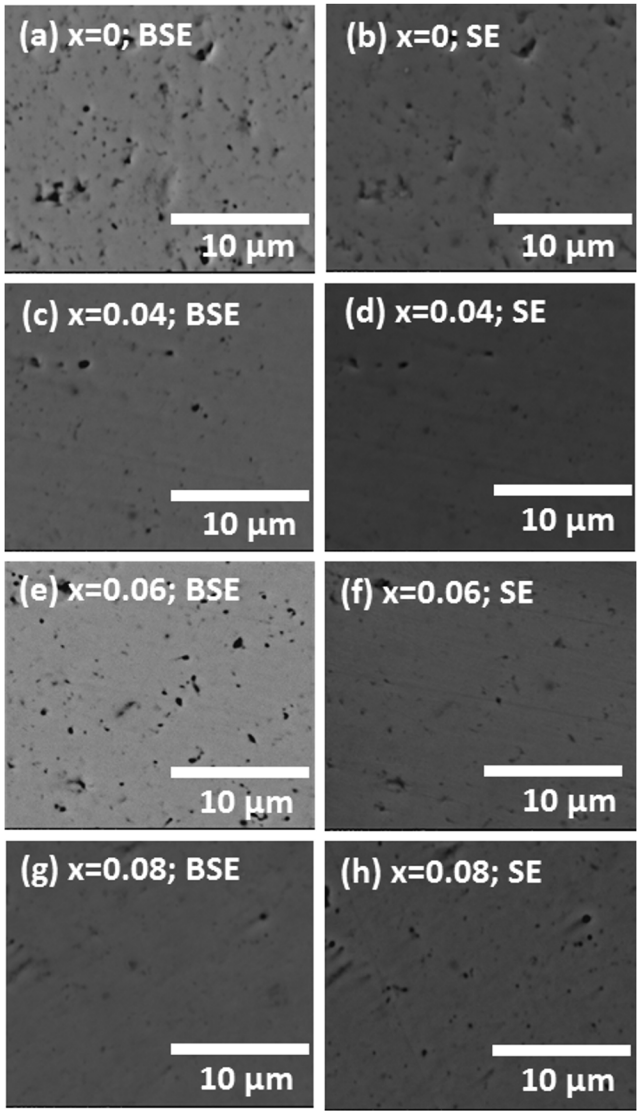

FIG. 3. (a) The back scattered electron (BSE) image of (a) $Bi_{0.985}Na_{0.015}CuSeO$ (c) $Bi_{0.945}Na_{0.015}Pb_{0.04}CuSeO$ (e) $Bi_{0.925}Na_{0.015}Pb_{0.06}CuSeO$ (g) $Bi_{0.905}Na_{0.015}Pb_{0.08}CuSeO$ The corresponding secondary electron (SE) image of (b) $Bi_{0.985}Na_{0.015}CuSeO$ (d) $Bi_{0.945}Na_{0.015}Pb_{0.04}CuSeO$ (f) $Bi_{0.925}Na_{0.015}Pb_{0.06}CuSeO$.

rest of the samples. The lowest Seebeck coefficient is the manifestation of highest carrier concentration among the samples because of the Mott's formula[11] $S = \frac{8\pi^2 k_B^2}{3eh^2} m^* T \left(\frac{\pi}{3n}\right)^{2/3}$ and the lowest electrical resistivity is due to its inverse relationship with the carrier concentration $\rho = 1/(ne\mu)$. The carrier concentration of the $Bi_{0.985}Na_{0.015}CuSeO$, $Bi_{0.945}Na_{0.015}Pb_{0.04}CuSeO$ and $Bi_{0.925}Na_{0.015}Pb_{0.06}CuSeO$ samples are $3.2\times10^{19}/cm^3$ $1.8\times10^{20}/cm^3$ and $4.5\times10^{20}/cm^3$ respectively. The carrier concentration of $Bi_{0.985}Na_{0.015}CuSeO$ sample is higher than the

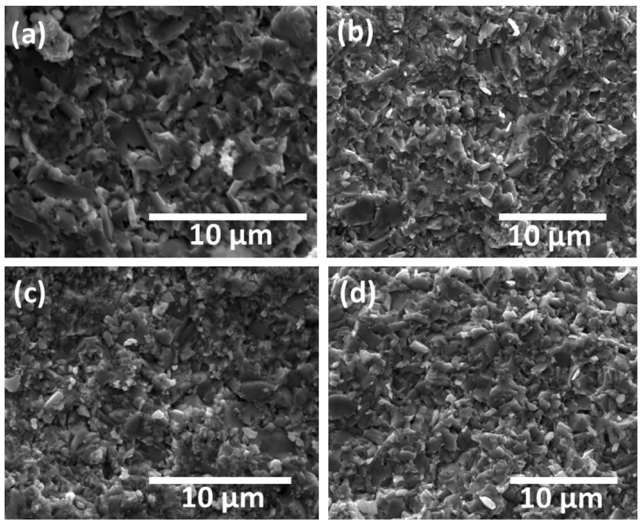

FIG. 4. The secondary electron (SE) image of the fractured surface of (a) $Bi_{0.985}Na_{0.015}CuSeO$ (b) $Bi_{0.945}Na_{0.015}Pb_{0.04}CuSeO$ (c) $Bi_{0.925}Na_{0.015}Pb_{0.06}CuSeO$ (d) $Bi_{0.905}Na_{0.015}Pb_{0.08}CuSeO$.

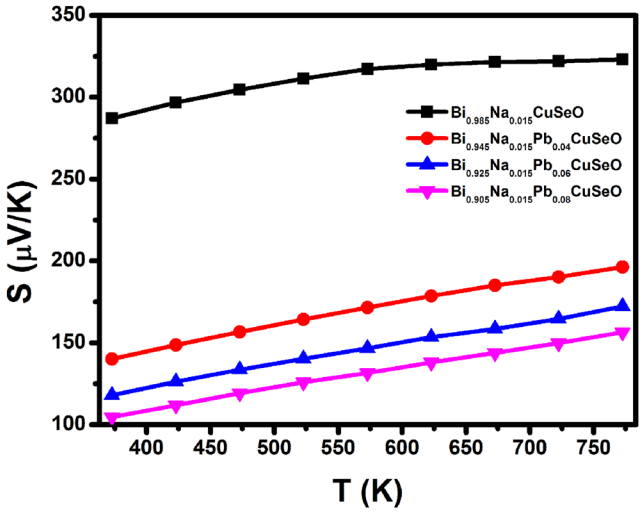

FIG. 5. Temperature dependence of Seebeck coefficient (*S*) of the $Bi_{0.985-x}Na_{0.015}Pb_xCuSeO$ (x=0, 0.04, 0.06 and 0.08) samples measured from 373 to 773 K.

pristine BiCuSeO (~2×10^{18} /cm^3)[12] as the Na^+ acts as an acceptor defect. The carrier concentration increases with increasing Pb doping fraction as Pb^{+2} also acts as an acceptor defect at the Bi site. The mobility of the $Bi_{0.985}Na_{0.015}CuSeO$, $Bi_{0.945}Na_{0.015}Pb_{0.04}CuSeO$ and $Bi_{0.925}Na_{0.015}Pb_{0.06}CuSeO$ are 10.28 cm^2/V-s, 10.21 cm^2/V-s and 5.78 cm^2/V-s respectively. Since this is a multi-phase system the mobility of the sample has contribution from both the secondary phase ($Bi_2O_{2.5}$) and main phase ($Bi_{0.985-x}Na_{0.015}Pb_xCuSeO$). As a result, the mobility calculated from the usual formula $\mu = 1/(ne\rho)$ does not reflect the true mobility of the main phase ($Bi_{0.985-x}Na_{0.015}Pb_xCuSeO$).

D. Transport properties

1. Seebeck coefficient (S)

The Seebeck coefficient (S) of the samples is shown in Figure 5. The positive S of the samples indicates that the holes are the majority charge carriers. The S decreases with increasing doping fraction indicating that holes are getting liberated in the system with Na and Pb doping. Lan *et al.*[4] have shown that the $6s^2$ lone pair electrons of Pb introduce states near the Fermi level. This enhancement of the density of states increases the effective mass of the holes, and in turn, positively affects the S, according to the Mott's formula.[13] Li *et al.* observed a higher S for the Na-doped BiCuSeO in comparison to the other dopants for the same carrier concentration.[6] They attributed this to the modification in the electronic structure due to Na doping. We did not observe a significant contribution of Na to the density of states (DOS) near the Fermi level from density functional theory as shown in Figure 6. However, the similar ionic radii of Na and Bi may have influence in the S, through maintaining the geometry of the Cu_2Se_2 layer. The linear geometry of the Cu_2Se_4 in $\left(\vec{a}+\vec{b}\right)$ and $\left(\vec{a}-\vec{b}\right)$ direction manifests itself in the one-dimensional characteristic in the DOS. This one-dimensional characteristic introduces sharp feature in the DOS which results in high S of BiCuSeO.[14] The

TABLE I. The Bi, Cu, Pb and Na content of the $Bi_{0.985-x}Na_{0.015}Pb_xCuSeO$ (x=0.0, 0.04,0.06 and 0.08) samples from EPMA (electron probe micro analysis).

Sample	Bi	Cu	Pb	Na
$Bi_{0.985}Na_{0.015}CuSeO$	0.971	1.000	0	0.005
$Bi_{0.945}Pb_{0.04}Na_{0.015}CuSeO$	0.925	1.000	0.044	0.003
$Bi_{0.925}Pb_{0.06}Na_{0.015}CuSeO$	0.908	1.000	0.061	0.003
$Bi_{0.905}Pb_{0.08}Na_{0.015}CuSeO$	0.884	1.000	0.069	0.001

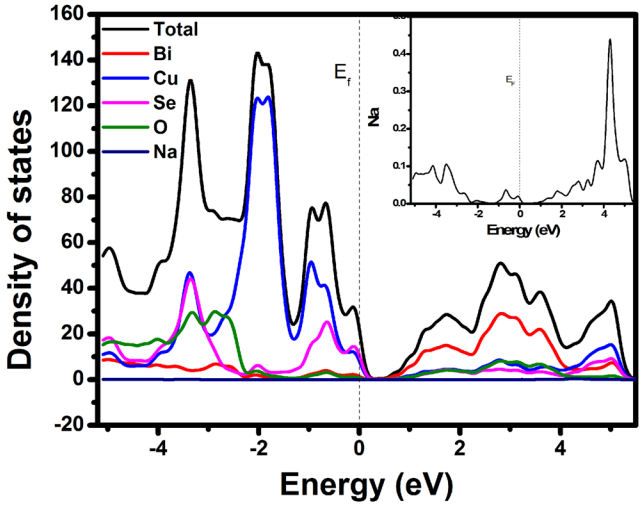

FIG. 6. Projected density of states of Na doped BiCuSeO. The projected density of states of Na is shown in the inset.

lattice distortion caused by the dopants at the Bi site may disrupt the linear geometry of the Cu_2Se_4 chain through the Bi 6p Se 4p orbital interaction, and thus the sharp feature in the DOS is lost. The similar ionic radii of Na and Bi maintains the structure of the Cu_2Se_4 chain, and thus the S of Na-doped samples is higher than the other dopants for the same carrier concentration. The S of $Bi_{0.985}Na_{0.015}CuSeO$ varies from 287 μV/K to 323 μV/K, throughout the temperature range (373-773 K), which is similar to the reported value of 270 μV/K to 309 μV/K in the same temperature range and same composition.[6] This is because of similar carrier concentration of both the samples. The S of the sample with x=0.04, 0.06, and 0.08 varies linearly with temperature, showing metallic characteristics, as the doping of Pb and Na shifts the Fermi level inside the valence band.

2. Electrical resistivity (ρ)

The electrical resistivity (ρ) of the samples is shown in Figure 7. The ρ of the samples decrease with increasing in doping fraction of Pb, liberate holes into the system since they act as acceptor defects at the Bi site. Although the charge reservoir in Bi_2O_2 layer is separated from the conduction channel of Cu_2Se_2, dopants at Bi site sharply reduces the hole mobility. For example, the hole-mobility of pristine BiCuSeO is ~10 cm^2/V-s, whereas the mobility of $Bi_{0.875}Ba_{0.125}CuSeO$ is ~2 cm^2/V-s.[3,4] The ionic nature of Na does not affect the charge carrier mobility as the bonding between Na-O may not affect the conduction channel. Pb doping is also advantageous for the hole mobility because of the delocalized $6s^2$ lone pair electrons.[4] The ρ of the $Bi_{0.985}Na_{0.015}CuSeO$ sample varies from 0.24-0.34 mΩ-m throughout the temperature range which is twice that of the reported value by Li *et al.* (0.110-0.185 mΩ-m). Although the S and n of both the samples is similar. This discrepancy in the ρ could be due to the presence of $Bi_2O_{2.5}$ oxide phase in the system. Unlike the Cu_xSe phase which can readily occur in BiCuSeO system,[13] the bismuth oxide phase has high resistivity, and hence, it can adversely affect the ρ of the samples.[15] The ρ of the samples decreases with increasing doping concentration, as Pb and Na act as acceptor defects. The samples with x=0.04,0.06 and 0.08 vary linearly with temperature showing a metallic characteristic, in agreement with the S. The lowest ρ has been achieved for the x=0.08 sample which varies from 0.022 -0.046 mΩ-m in the measured temperature range.

3. Thermal conductivity (κ)

The total thermal conductivity (κ) of the samples which is the sum of the lattice part κ_L and the electronic part (κ_e) of thermal conductivity is shown in Figure 8. The κ_e was calculated by the Wiedemann-Franz relation-

$$\kappa_e = LT/\rho, \tag{2}$$

where L is the Lorenz number. The Lorenz number was calculated assuming acoustic phonon scattering and single parabolic band conduction[16] using the following formula-

$$L = \frac{k_B^2}{e^2}\frac{3F_0(\eta)F_2(\eta) - 4F_1^2(\eta)}{F_0^2(\eta)}, \tag{3}$$

where η is the reduced Fermi energy (E_F/k_BT), $F_n(\eta)$ is the nth order Fermi function. The reduced Fermi energy was found out by fitting the Seebeck coefficient. The κ_L (depicted in Figure 9) was obtained by the formula $\kappa_L = \kappa - \kappa_e$. The κ_L of the samples decreases with increasing temperature, because of the increase in the phonon-phonon Umklapp scattering at high temperatures. The decrease in κ_L is gradual in nature from x=0.0 to 0.06. Pb and Bi have almost similar atomic mass, of 207.2 amu and 208.9804 amu respectively. The delocalized lone pair electrons of Pb does not have much effect on the bond-anharmonicity as the repulsion of the lone pairs on the other bonds is less.[4,17] As a result, the doping of Pb does not

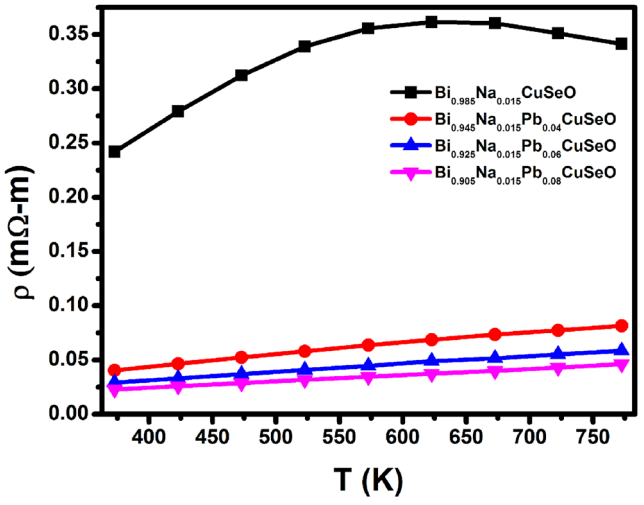

FIG. 7. Temperature dependence of the electrical resistivity (ρ) of the $Bi_{0.985-x}Na_{0.015}Pb_xCuSeO$ (x=0.0, 0.04,0.06 and 0.08) samples measured from 373 to 773 K.

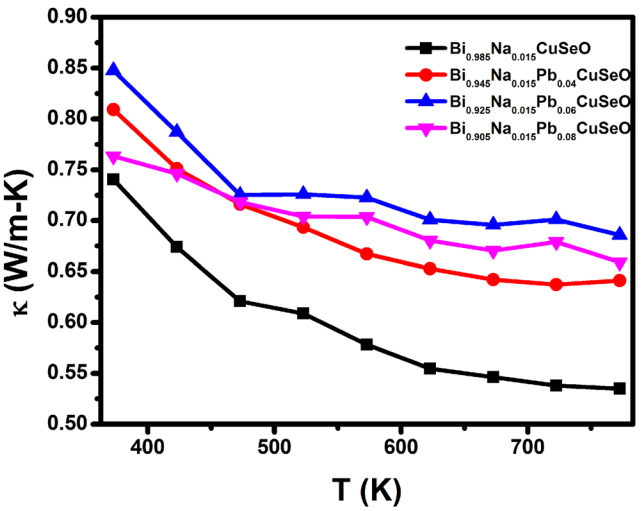

FIG. 8. Thermal conductivity (κ) of the $Bi_{0.985-x}Na_{0.015}Pb_xCuSeO$ (x=0.0, 0.04,0.06 and 0.08) samples as a function of temperature.

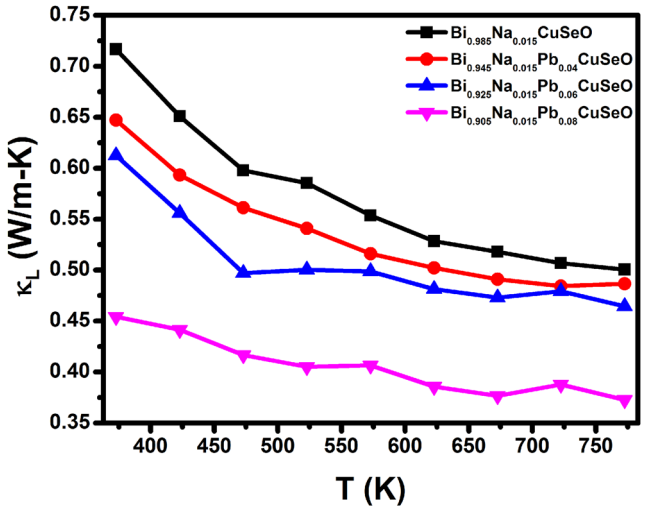

FIG. 9. The lattice thermal conductivity (κ_L) of the $Bi_{0.985-x}Na_{0.015}Pb_xCuSeO$ (x=0.0, 0.04,0.06 and 0.08) samples as a function of temperature.

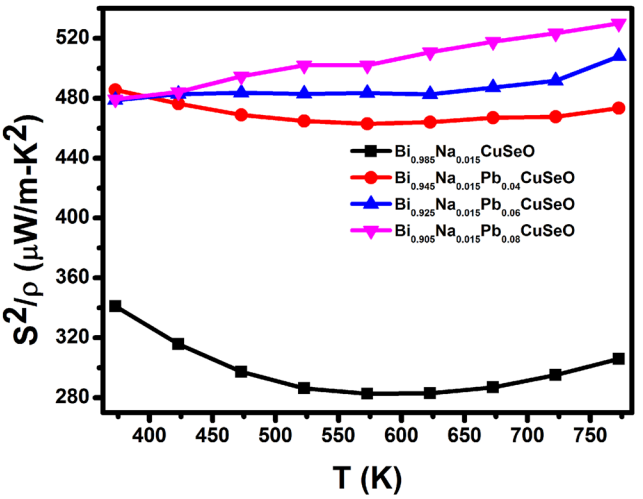

FIG. 10. The temperature dependence of the power factor (S^2/ρ) of the $Bi_{0.985-x}Na_{0.015}Pb_xCuSeO$ (x=0.0, 0.04,0.06 and 0.08) samples.

lead to heavy mass fluctuation scattering or increase the bond anharmonicity. Due to this fact, the decrease in κ_L on doping of Pb is only due to the size defect scattering, and the resulting reduction in κ_L is very less. The sharp fall in the κ_L of the sample with x=0.08 can be explained by the formation of nanoprecipitates in the system at the onset of solubility limit of Pb. Nano-precipitation of CuSe with sizes 5-10 nm has been observed in high-resolution transmission electron microscope at high doping fraction (≥6 at. %) by Lan *et al.* [4]as well as Ren *et al.*[18] Nano precipitations scatter the phonons through boundary scattering. Above Debye temperature (θ_D), the Umklapp scattering is more significant than the boundary scattering. However, particles below 10 nm can impede the phonons even at higher temperatures because of the significant contribution from the phonons which have mean free path more than 10 nm even at high temperatures.[19] Thus, the κ_L of x=0.08 is far less than the rest of the samples throughout the temperature range which could be due to nano-precipitation inside the BiCuSeO matrix.

E. Power factor (S^2/ρ) and dimensionless figure of merit (*z*T)

The power factor (S^2/ρ) is shown in Figure 10. Due to low ρ and moderate S, the highest power factor of 530 μW/m-K^2 was obtained for x=0.08 at 773 K. While this S^2/ρ is more than Mg-doped BiCuSeO (~200 μW/m-K^2 at 773 K)[20] it is less than the Ca and Pb dually doped BiCuSeO (~800 μW/m-K^2 at 773 K).[5] Notably, the variation of S^2/ρ for the $Bi_{0.905}Na_{0.015}Pb_{0.08}CuSeO$ sample is small ranging from 480 to 530 μW/m-K^2 throughout the temperature range which is beneficial for having a high average zT. This high average zT can enhance the device efficiency, as the device efficiency depends on the average zT between the hot and the cold side temperature. The zT of the samples is shown in Figure 11. The highest zT of 0.63 at 773 K was obtained for $Bi_{0.905}Na_{0.015}Pb_{0.08}CuSeO$ due to high S^2/ρ and low κ_L. The nanoparticles reduce the lattice thermal conductivity. Doping on the other hand, reduces the electrical resistivity, and the electrical resistivity of the sample with x=0.08 has the lowest electrical resistivity among all other sample (0.022 -0.046 mΩ-m in the measured temperature). As a result, the highest power factor of the was achieved sample with x=0.08 (530 μW/m-K^2 at 773 K). This lowest electrical resistivity and the highest power factor is achieved because of doping at the Bi site (both Na and Pb). This zT is higher than quite a few singly doped BiCuSeO like Mg-doped BiCuSeO (~0.5 at 773 K),[19] Mn-doped BiCuSeO (~0.4 at 773 K)[21] or Ag-doped BiCuSeO (~0.55 at 773 K).[22] However, it is lower than many

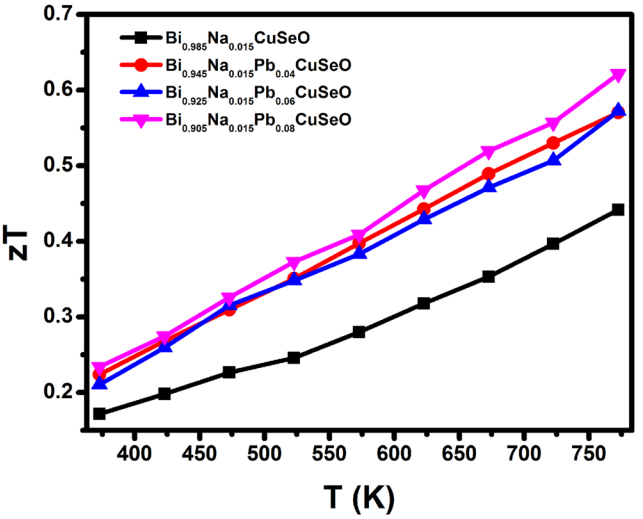

FIG. 11. Dimensionless figure of merit (zT) of the $Bi_{0.985-x}Na_{0.015}Pb_xCuSeO$ (x=0.0, 0.04,0.06 and 0.08) samples as a function of temperature.

of the dually-doped BiCuSeO for example- Ca and Pb dually doped BiCuSeO (~1.2 at 773 K),[5] Pb/Te co-doped BiCuSeO (~1 at 773 K)[23] and Fe/Pb dually doped BiCuSeO (~1.3 at 773 K).[24] In comparison to the other dually doped BiCuSeO, the zT is lower in this report because of the presence of impurity phase of bismuth oxide which increases the electrical resistivity and adversely affects the zT.

V. CONCLUSIONS

In summary, the thermoelectric properties of Na and Pb dually doped BiCuSeO with composition $Bi_{0.985-x}Na_{0.015}Pb_xCuSeO$ (x=0.00, 0.04, 0.06 and 0.08) were studied. Na was doped along with Pb at the Bi site to increase the hole concentration without deteriorating the mobility of holes. An impurity phase of $Bi_2O_{2.5}$ was found for all the samples, which adversely affects the ρ. S and ρ decreased with increasing doping fraction due to the generation of holes. Although Na does not introduce states near the Fermi level, the similarity in the ionic radii of Bi and Na can be favorable for increasing the S. A sharp fall in the κ_L was observed for x=0.08. Due to the low κ_L of 0.37 W/m-K and a high power factor of 530 $\mu W/m\text{-}K^2$ at 773 K, a maximum zT of 0.63 was obtained for x=0.08 at the same temperature. The zT can be further improved by eliminating the impurity phase.

ACKNOWLEDGMENTS

We would like to thank Ms. Sanyukta Ghosh for measuring the electrical transport properties. We would also like to thank SERC, IISc. for providing the computational facility.

REFERENCES

[1] C. Barreteau, D. Berardan, and N. Dragoe, J. Solid State Chem. **222**, 53 (2015).
[2] L. D. Zhao, J. He, D. Berardan, Y. Lin, J. F. Li, C. W. Nan, and N. Dragoe, Energy Environ. Sci. **7**, 2900 (2014).
[3] J. Li, J. Sui, Y. Pei, C. Barreteau, D. Berardan, N. Dragoe, W. Cai, J. He, and L. D. Zhao, Energy Environ. Sci. **5**, 8543 (2012).
[4] J. Le Lan, Y. C. Liu, B. Zhan, Y. H. Lin, B. Zhang, X. Yuan, W. Zhang, W. Xu, and C. W. Nan, Adv. Mater. **25**, 5086 (2013).
[5] Y. Liu, L. D. Zhao, Y. Zhu, Y. Liu, F. Li, M. Yu, D. B. Liu, W. Xu, Y. H. Lin, and C. W. Nan, Adv. Energy Mater. **6**, 1502423 (2016).
[6] J. Li, J. Sui, Y. Pei, X. Meng, D. Berardan, N. Dragoe, W. Cai, and L. D. Zhao, J. Mater. Chem. A **2**, 4903 (2014).
[7] S. Das, A. Ramakrishnan, K. H. Chen, D. K. Misra, and R. C. Mallik, J. Phys. D. Appl. Phys. **51**, 35501 (2018).
[8] J. Rodríguez-Carvajal, Phys. B Phys. Condens. Matter **192**, 55 (1993).
[9] P. Giannozzi, S. Baroni, N. Bonini, M. Calandra, R. Car, C. Cavazzoni, D. Ceresoli, G. L. Chiarotti, M. Cococcioni, I. Dabo, A. Dal Corso, S. de Gironcoli, S. Fabris, G. Fratesi, R. Gebauer, U. Gerstmann, C. Gougoussis, A. Kokalj, M. Lazzeri, L. Martin-Samos, N. Marzari, F. Mauri, R. Mazzarello, S. Paolini, A. Pasquarello, L. Paulatto, C. Sbraccia, S. Scandolo, G. Sclauzero, A. P. Seitsonen, A. Smogunov, P. Umari, and R. M. Wentzcovitch, J. Phys. Condens. Matter **21**, 395502 (2009).
[10] R. D. Shannon, Acta Crystallogr. A **32**, 751 (1976).
[11] M. Cutler, J. F. Leavy, and R. L. Fitzpatrick, Phys. Rev. **133**, A1143 (1964).
[12] S. Das, A. Ramakrishnan, K.-H. Chen, D. K. Misra, and R. C. Mallik, J. Electron. Mater.Submitted (2018).
[13] S. Das, R. Chetty, K. Wojciechowski, S. Suwas, and R. C. Mallik, Appl. Surf. Sci. **418**, 238 (2017).
[14] C. Lee, T.-H. An, E. E. Gordon, H. S. Ji, C. Park, J.-H. Shim, Y. S. Lim, and M.-H. Whangbo, Chem. Mater. **29**, 2348 (2017).
[15] F. Li, J. F. Li, L. D. Zhao, K. Xiang, Y. Liu, B. P. Zhang, Y. H. Lin, C. W. Nan, and H. M. Zhu, Energy Environ. Sci. **5**, 7188 (2012).
[16] H.-S. Kim, Z. M. Gibbs, Y. Tang, H. Wang, and G. J. Snyder, APL Mater. **3**, 041506/1 (2015).
[17] E. J. Skoug and D. T. Morelli, Phys. Rev. Lett. **107**, 235901 (2011).
[18] G.-K. Ren, J. Lan, S. Butt, K. J. Ventura, Y.-H. Lin, and C.-W. Nan, RSC Adv. **5**, 69878 (2015).
[19] S. Kumar and U. Schwingenschlogl, Phys. Chem. Chem. Phys. **18**, 19158 (2016).
[20] J. Li, J. Sui, C. Barreteau, D. Berardan, N. Dragoe, W. Cai, Y. Pei, and L. D. Zhao, J. Alloys Compd. **551**, 649 (2013).
[21] S. Das, S. Meledath Valiyaveettil, K.-H. Chen, S. Suwas, and R. C. Mallik, Mater. Res. Express (2018).
[22] M. U. Farooq, S. Butt, K. Gao, X. L. Pang, X. Sun, Asfandiyar, F. Mohmed, A. Ahmad, A. Mahmood, and N. Mahmood, J. Alloys Compd. **691**, 572 (2017).
[23] G. K. Ren, S. Y. Wang, Y. C. Zhu, K. J. Ventura, X. Tan, W. Xu, Y. H. Lin, J. Yang, and C. W. Nan, Energy Environ. Sci. **10**, 1590 (2017).
[24] X. Zhang, D. Feng, J. He, and L.-D. Zhao, J. Solid State Chem. **258**, 510 (2018).